ISET Journal of Earthquake Technology, Paper No. 414, Vol. 38, No. 2-4, June-Dec. 2001, pp. 103-122

A COMPARATIVE STUDY OF BRICK MASONRY HOUSE MODEL UNDER QUASI-STATIC AND DYNAMIC LOADING

Pankaj Agarwal* and S.K. Thakkar**

* Lecturer ** Professor

Department of Earthquake Engineering

Indian Institute of Technology Roorkee, Roorkee – 247 667

ABSTRACT

Quasi-static tests on structural models have often been conducted with the objective to study hysteresis behaviour of the structure under prescribed loading and to determine the capacity of the structure such as maximum resistance and ductility. It has not yet been established how the results of these tests may be compared with dynamic test results. In this paper, a comparative study of behaviour of two half-scaled brick masonry house models have been made which are constructed with similar earthquake resistance features. Two types of tests are conducted on the models: shock table test and quasi-static test (QST). The shock table test consists of applying an impact type of loading in a shock table facility that produces nearly a half-sine pulse type of motion at the base of the platform carrying the model. The quasi-static test consists in applying a cyclic load at roof level at a very low frequency. The criterion for comparison of both the tests is the maximum absolute displacement at the roof level. The shock table model responds with a significant higher initial strength and stiffness as compared to the quasi-static model. The severity of damage is greater in quasi-static test due to increased crack propagation, thus proving conservatism of quasi-static test.

KEYWORDS: Shock Table Test, Quasi-static Test, Brick Masonry, Hysteresis Behaviour

INTRODUCTION

Brick masonry is the oldest building material. Inspite of this, the technological development of masonry in earthquake engineering has lagged behind compared to other structural materials like concrete and steel. The paucity of knowledge on the subject has led to a lack of confidence by engineers with regard to its use in seismic environment. The last three decades have bestowed on us a significant knowledge of earthquake engineering regarding seismic analysis, design and experimental testing facility. Advances in servo-hydraulic technology and computer simulation are making actual shaking more feasible in earthquake engineering, but fundamentally, such researches are being concentrated principally on steel and concrete structures whereas majority of population in India lives in low-strength masonry houses constructed with stone, brick, mud, adobe, etc. Research work has often been carried out on small scale models either under horizontal static loading or dynamic loading to understand the behaviour of masonry walls and buildings (Krishna and Chandra, 1965; Qamaruddin et al., 1978; Arya and Kumar, 1982; Clough et al., 1979; Tomazevic and Velechorsky, 1992). These investigative programmes have led to the results regarding development of methods for seismic resistance, analysis and design as well as new seismic resistant technology and construction techniques. It is not yet known, to what extent the observations from static test can be correlated with dynamic test in terms of strength, stiffness and mode of failure (Benedetti and Castellani, 1982). An attempt has been made here to study the behaviour of two brick masonry models constructed with identical features under shock table testing and quasi-static testing (Agarwal, 2000). Shock table testing is a dynamic method of testing where base motion is given by impact. This impact imparts horizontal shocks in the form of sine pulse to the foundation sufficient to destroy the structure. The quasi-static test is not a dynamic test; in that, the rate of application of the load is low and inertia forces do not develop. The loading pattern and history must be general, and enough to provide the full range of these deformations that the structure will experience under the earthquake excitations. This method adequately captures the important dynamic

characteristics of the structure, i.e. hysteresis behaviour, energy dissipation capacity, stiffness degradation, ductility, hysteretic damping, the most distressed regions, lateral strength and deformation capacity. This experimental data is utilised to make the complex hysteretic model for carrying out the dynamic analysis of structure. This paper is focused on the behaviour of brick masonry house model under dynamic and static condition, to suggest differences in strength, stiffness and mode of failure.

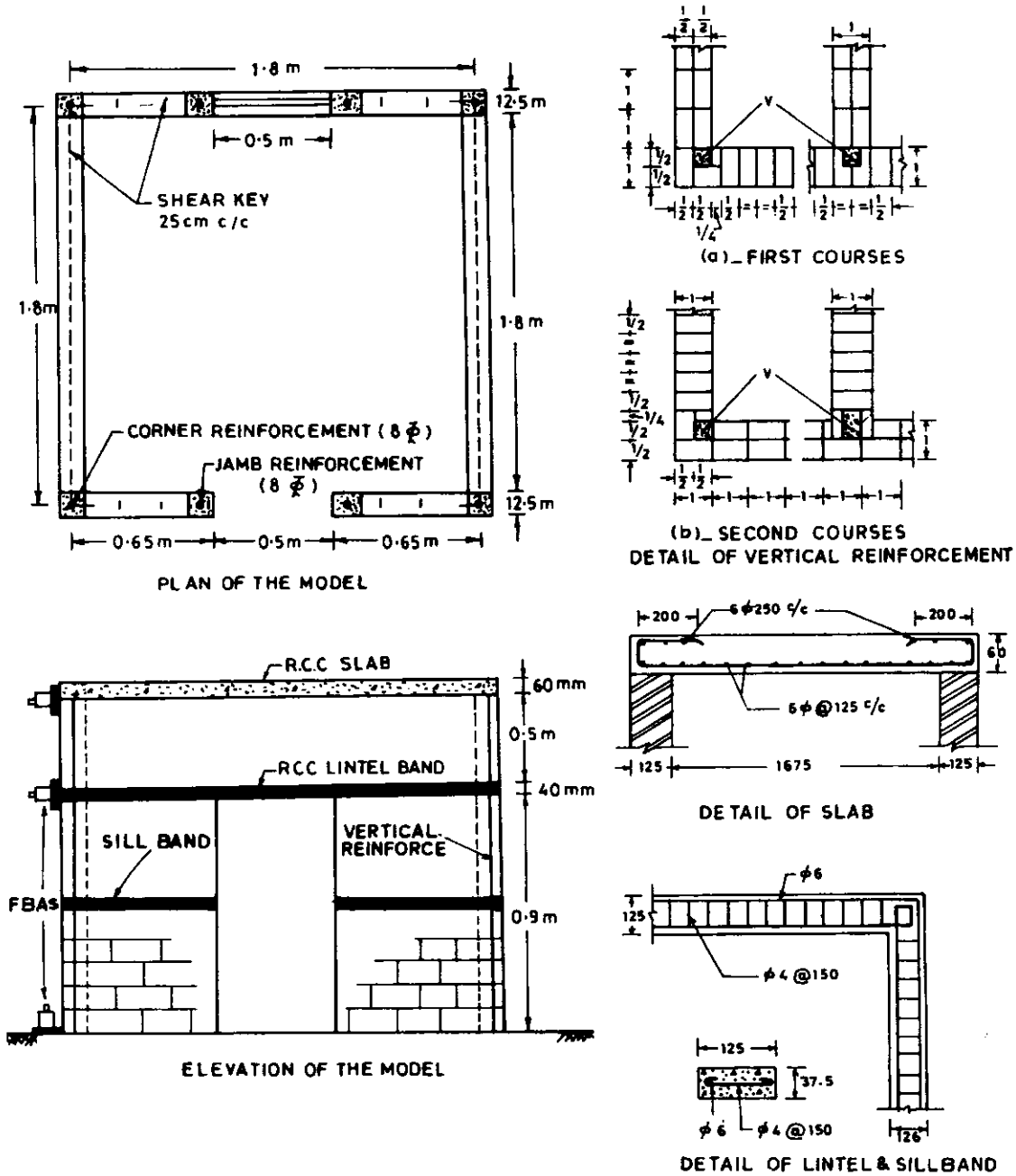

Fig. 1 Layout plan and elevation of model with details of reinforcements

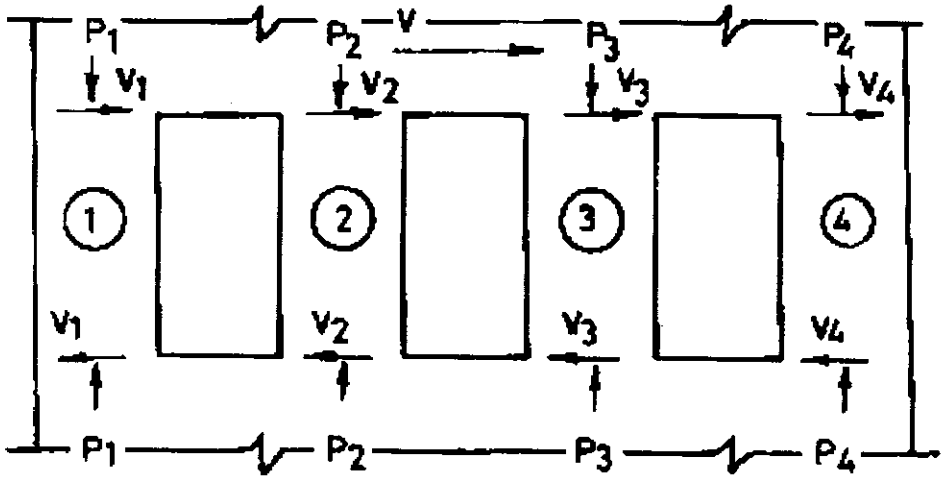

(a) WALL WITH OPENINGS

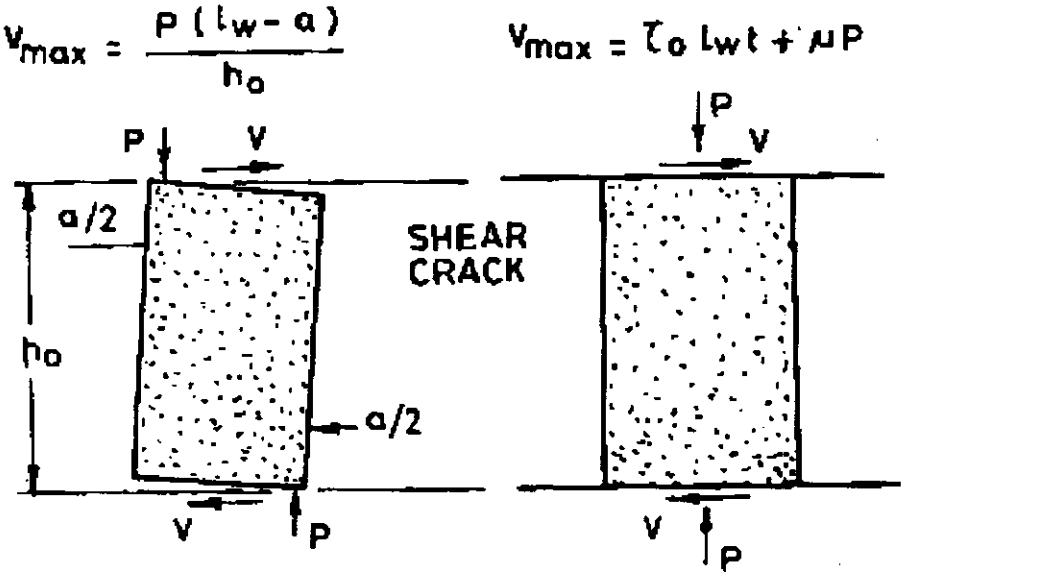

(b) ROCKING PIER (c) SHEAR FAILURE OF PIER

Fig. 2 Failure of unreinforced wall with piers

FEATURES OF BRICK MASONRY MODELS

1. Test Model

Two half-scale single room models of similar size with same earthquake resistant measures have been constructed for testing on shock table and in quasi-static test facility. The characteristics of prototype structure have been incorporated as far as possible in the models. The size of the model is determined on the basis of permissible payload of the table (20 tonnes). The plan size of the models is 1.8 x 1.8 m which are made on a steel base plate connected to the platform with shear keys. The height of each model and thickness of walls is 1.5 m and 0.125 m, respectively. The models have been constructed with 1:6 cement-sand mortar; the roof consists of reinforced concrete slab of thickness 8 cm. The bricks used for the construction of models are half-full size, i.e. 12 x 6 x 4 cm. The shear walls with door and window openings have been oriented in the direction of application of load. The main earthquake resistant features in the models consist of a roof slab, lintel band, and sill band and vertical reinforcement of 8 mm diameter at wall intersections as well as at window and door openings. The reinforcing bars have been anchored into bottom steel plate. The details of earthquake resistant measures have been provided according to IS 13928 (1993). The layout plan and elevation of the models with details of reinforcement are given in Figure 1.

2. Lateral Load Capacity of Model

The maximum lateral load capacity of unreinforced wall subjected to in-plane excitation has been determined (Paulay and Priestley, 1992) by dividing the shear walls into two piers by openings (Figure 2). The maximum shear force (lateral load) that can be transmitted by a typical pier could be either in a rocking mode or in shear failure mode.

For a rocking mode, the maximum shear force is,

$$V = P(l_w - a)/h_0 \tag{1}$$

where, a is the compression contact length at ultimate, i.e. $a = P/(0.85 f'_m t)$ and f'_m = compressive strength of masonry.

The maximum shear force (lateral load) that can be transmitted by a typical pier in shear failure mode is computed as

$$V = \tau_0 l_w t + \mu P \tag{2}$$

where, P = axial load, l_w = width of piers, t = thickness of wall, τ_0 = mean shear strength of masonry, and μ = coefficient of friction which may vary with test method and type of masonry. The typical range of values are $0.3 \leq \mu \leq 1.2$. Since there is no external axial load, the second term in Equation 2 is neglected. Therefore, the shear capacity of wall is,

$$V = \tau_0 l_w t \tag{3}$$

The mean shear strength (τ_0) without any compressive load has been obtained by testing specially prepared specimens.

The approximate lateral load capacity of unreinforced model for 1:6 cement sand mortar in the shear mode is 65 kN.

3. Strength and Elastic Properties of Brick Masonry

It is difficult to determine the elastic properties of masonry on the basis of known properties of the constituent materials, e.g. masonry units and mortars. A series of model wall specimens have been constructed and tested by subjecting them either to vertical compression or combination of constant vertical and cyclic lateral loading. The following tests have been performed to determine the characteristic values of brick masonry (Drysdale et al., 1994):

(i) compressive strength

(ii) tensile and shear strength

(iii) modulus of elasticity

Table 1: Properties of Brick Masonry Column (1:6 Cement Sand Mortar)

Compressive Strength Test				
Specimen Dimension (mm)			**Ultimate Load (kN)**	**Ultimate Strength (N/mm^2)**
width	*thickness*	*height*		
200	200	450	95.00	2.375
200	200	450	100.50	2.512
200	200	450	96.50	2.412
			Average Strength (N/mm^2)	**2.433**
Tensile and Shear Strength Test (Racking Test Method)				
Specimen Dimension (mm)			**Shear Strength (N/mm^2)**	**Tensile Strength (N/mm^2)**
width	*thickness*	*height*		
500	120	600	0.167	0.251
500	120	600	0.208	0.312
500	120	600	0.224	0.336
500	120	600	0.207	0.310
		Average	**0.200**	**0.300**

Modulus of Elasticity of Brick Masonry Column (Static Test)						
Specimen Dimension (mm)			**Ultimate Pull (kN)**	**Deformation (mm)**	**Stiffness (N/mm)**	**E (N/mm^2)**
width	*thickness*	*height*				
200	200	600	0.27	2.48	108.9	58.90
200	200	600	0.30	2.55	117.6	63.66
200	200	200	0.40	1.98	201.5	109.08
					Average	**77.21**

Modulus of Elasticity of Brick Masonry Column (Free Vibration Test)						
Specimen Dimension (mm)			**Frequency (Hz)**	**Mass Density (t/m^2)**	**E (N/mm^2)**	**Damping %**
width	*thickness*	*height*				
200	200	600	28.15	1.92	192.56	3.64
200	200	600	22.65	1.92	124.66	2.00
200	200	200	26.22	1.92	167.07	2.82
				Average	161.43	2.82

The compressive strength of masonry has been obtained by testing standard prisms that usually are one masonry unit long, one unit thick and can be built to the limit of various heights between 1.5 to 5 times the thickness (ASTM: E 447-84, 1984). Three brick masonry columns built from half full-size bricks were constructed with 1:6 cement sand mortar of size 200x200x450 mm. All these specimens have been tested in quasi-static test facility. Compressive force has been controlled by a load cell during the process of testing, while the deformations in masonry have been measured by LVDTs in longitudinal and transverse directions. The average value of the compressive strength of brick masonry in 1:6 cement sand mortar has been obtained.

The ASTM describes two test methods for determining the tensile strength of brick masonry: the diagonal compression test and a racking test (ASTM: E72, 1989). In racking method of testing, a square wall panel is subjected to a horizontal force at the top of wall. An axial load can be included. Vertical restraint by a tie-down is required to prevent overturning of the specimen. To obtain tensile strength of brick masonry model, three wall specimens of size 0.6x0.6x0.12 m were prepared and fixed on the floor. Top end of the wall was compressed by steel plate through bolts and nuts so that the wall failed in shear. The lateral load

was applied by the hydraulic actuator at the other top end of the specimen. The principal tensile stress at failure (f_t) may be calculated from the equations proposed by Turnsek and Cacovic (1970), while neglecting horizontal normal stress

$$f_t = \sqrt{(1.5\tau_0)^2 + (0.5\sigma_0)^2} - 0.5\sigma_0 = 1.5\tau_k \quad (4)$$

$$\tau_0 = \tau_k \sqrt{1 + (\sigma_0 / 1.5\tau_k)} \quad (5)$$

where, τ_k is the principal tensile stress at failure divided by 1.5. Equation 4 gives the higher values of τ_k in the absence of vertical load.

The flexural modulus of elasticity has been determined by quasi-static testing of brick masonry columns of size 200x200x600 mm as vertical cantilevers under lateral load. The modulus of elasticity has also been determined with the aid of free vibration records.

The results of the above tests have been evaluated and are presented in Table 1.

SHOCK TABLE TESTING OF MODEL

1. Shock Table Test Facility

Keightly (1972) developed shock table facility for conducting dynamic tests on a low-grade masonry house extended up to the weight of twenty tonnes at a considerably low cost. This facility is suitable for studying the relative merits of different earthquake resistance measures in structural models and for conducting feasibility studies on new concepts of earthquake resistance measures. This consists of following component: (i) track or permanent way, (ii) shock table, (iii) dead load wagons or striking wagons and, (iv) winch mechanism to pull wagons.

The track consists of three lengths of 12 m each, spiked to sal wood sleepers placed at a space of 750 mm. The rails are demarcated at an interval of half meter for directing and guiding the positioning of the wagons before an impact. A rigid steel platform of 7x6 m forms a shock table for conducting dynamic tests on structural models. Ten helical coil compression springs have been mounted around pipe pieces and welded on each end of the platform to help to moderate the impact. The loaded wagons have been placed on the track on both sides of the shock table. One of the loaded wagons is allowed to roll down the gentle incline, give impact through springs, and thus to drive the table into collision with the other dead load wagon, which remains temporarily at rest. Single shock from end wagon imparts half-sine type of pulse to central wagon. When the other wagon is used to take reaction, it can impart another half-sine pulse from rebound. In this way, one impact of end wagon can produce series of half-sine pulses. The general arrangement of the shock table and its signature of shock are given in Figure 3.

2. Shock Test Results

2.1 Instrumentation and Data Acquisition

The model was instrumented with three unidirectional force balance accelerometers (FBA-11) to measure the absolute accelerations at the top (a_T), lintel level (a_L) and the bottom (a_g) of the model mounted on the table in the direction of horizontal motion. The summary of test results has been presented in Table 2. The response quantities in Table 2 are maximum values and may not have necessarily occurred at the same instant of time. The lateral drift (d_T/H) is the maximum top level deflection divided by total height H. The approximate lateral force (F_T) at each shock has been calculated as the product of roof acceleration times mass (85% of total mass of model) associated with roof level (Paulson and Abrams, 1990). The natural frequency and coefficient of equivalent viscous damping of model have been determined by analysing the free vibration records of model before and after the testing. Seismometers and solid state

recorder have recorded the free vibration response. Natural frequency of the original model is about 6 Hz and damping lies in the range of 3 to 4%. After damage, a decrease in frequency (2.8 Hz) and an increase in damping (8%) has been observed.

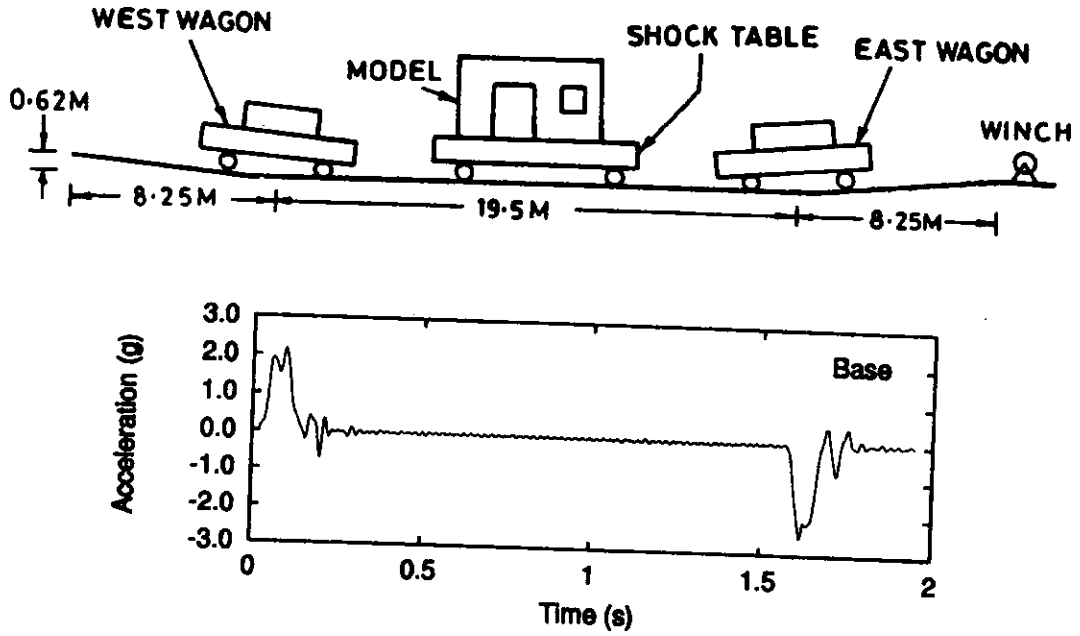

Fig. 3 Shock table facility and its signature of shock

Table 2: Summary of Test Results for Shock Table Testing of Model

Shock No.	Acceleration (g) at			Amplif-ication	Defor-mation	Lateral Drift	Eq. Lateral Force	Stiffness	Freq-uency	Damp-ing
	base	*lintel*	*roof*	-	*roof*	%	*kN*	*kN/mm*	*(Hz)*	*(%)*
	a_g	a_L	a_T	a_T/a_g	d_T	d_T/H	F_T	K	f	ξ
Shock 1 (W-19)	1.470	1.75	1.92	1.30	12.78	0.91%	40	3.12	5.82	3.40
Shock 2 (W-20)	1.753	2.25	2.50	1.42	15.53	1.08%	48.2	3.10	-	-
Shock 3 (W-21)	2.307	-	2.86	1.24	17.46	1.24%	46.0	2.75	2.80	8.65

2.2 Acceleration Pattern and Inelastic Behaviour of Model

The model has been subjected to three shocks. The typical acceleration time-history under different shocks on models is shown in Figure 4. The linear elastic response spectra of base shocks are shown in Figure 5. The intensity of each test run has been increased progressively. At low excitation, i.e. Shock 1 (W-19), base acceleration is magnified by a factor of about 1.3 times at the roof level and this amplification tends to increase up to 1.42 as the test structure is subjected to Shock 2 (W-20). When the model has been subjected to shock 3 (W-21), the amplification factor gets reduced to 1.25. This indicates that the damaged

lower part of the model in previous shocks has functioned as a kind of base isolator, which prevents propagation of energy into upper portion of structure.

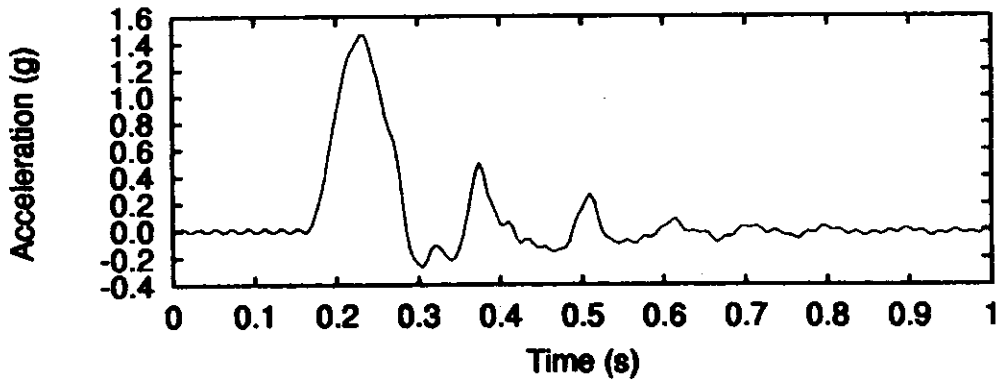

Shock table motion under W-19

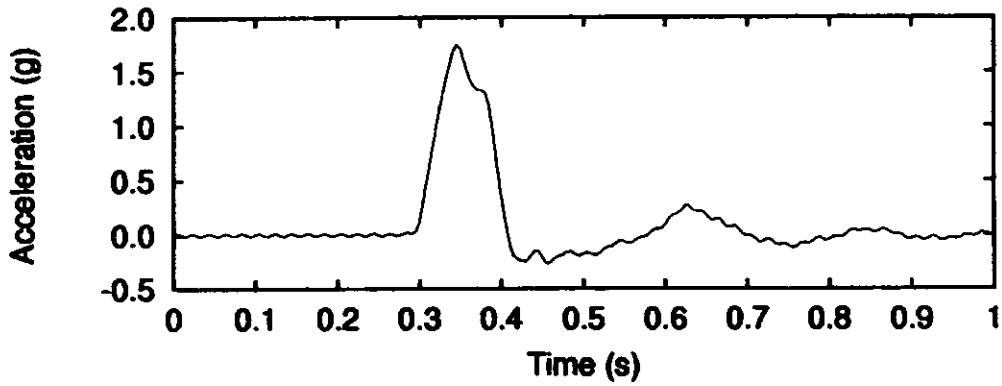

Shock table motion under W-20

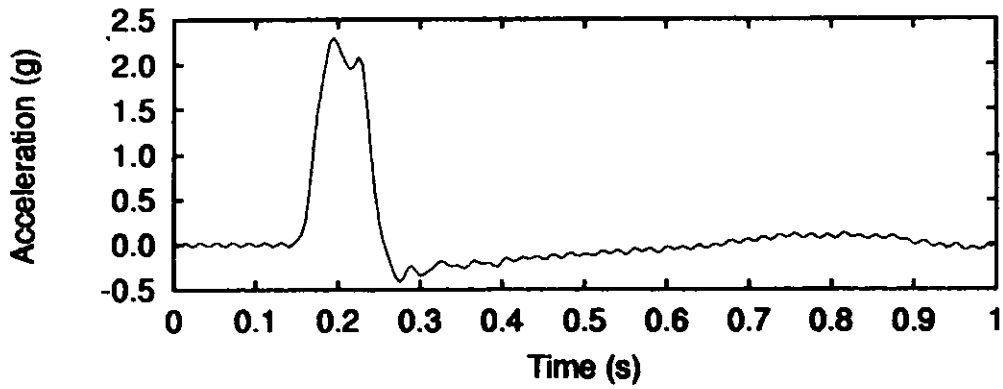

Shock table motion under W-21

Fig. 4 Signatures of shock table motion at different intensities

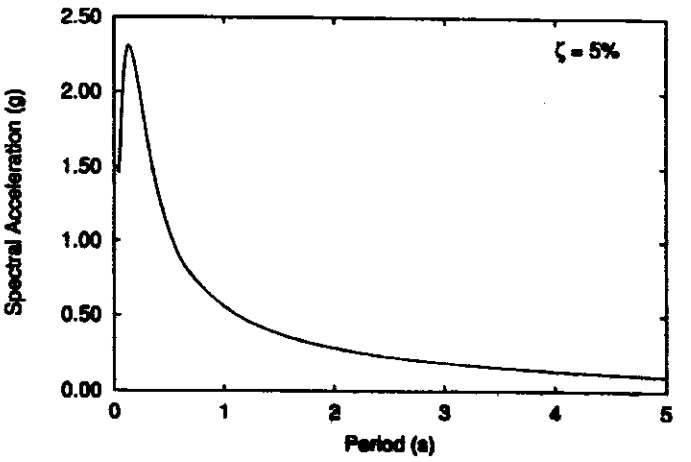

Response spectrum for shock W-19

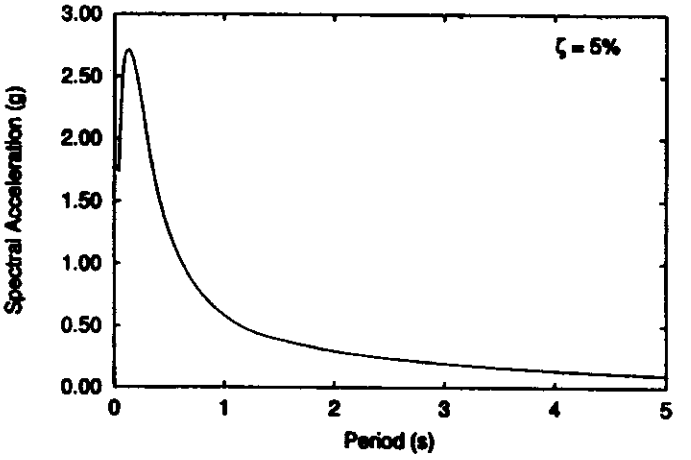

Response spectrum for shock W-20

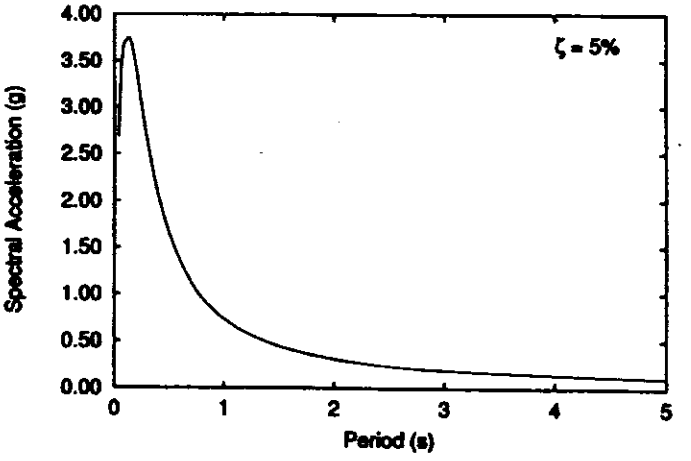

Response spectrum for shock W-21

Fig. 5 Linear elastic response spectra of shocks at different intensities

The main observations regarding the behaviour of the tested model are as follows. As a result of the first shock (W-19), a little damage to the model took place. Small, hardly visible cracks developed in the shear walls of the model. Although a few flexural cracks were observed in transverse walls, the width of cracks was insignificantly small. During the second test run (W-20), diagonal cracks were developed in the piers of shear walls between lintel and sill bands. There was no significant damage observed above the lintel band and below the sill band. The third and final shock (W-21) produced excessive shear, which resulted in in-plane shear failures of the piers between lintel and sill bands. The cracks propagated on both sides from door and window corners diagonally towards the top and bottom corners of model (brittle shear failure). Horizontal cracks developed in middle part of north shear wall below sill level, and propagated diagonally upwards and downwards. The initial cracks developed in previous shocks in piers of south shear wall below the sill band opened up under this shock and spread all over the pier diagonals (ductile shear failure). The out-of-plane vibration of transverse walls of the model was not observed even after increased intensity of motion during Shock 3 (W-21). This is possibly because of lintel and sill bands. Only a horizontal crack developed below the sill level where the excessive flexure stress developed. The test results indicate that out-of-plane seismic performance of wall piers may be considerably improved by the provision of bands at lintel and sill levels.

2.3 Correlation of Shock Table Motion with Actual Ground Motion

The shock table motion is basically an impulse type of motion with the characteristics as low duration, high base acceleration and high frequency content as against the actual ground motion. It is difficult to extrapolate structural behaviour under real earthquake motion from shock table tests. However, the intensity of damage of the shock can be compared with that in the earthquake motion by considering the effects of peak base acceleration, strong motion duration and frequency content simultaneously. Following are the parameters commonly used to characterize the intensity of damage of strong shaking (Uang and Bertero, 1988; Meskouris, 1996).

Peak ground acceleration is the most common parameter to describe the intensity and damage potential of an earthquake because the inertia force depends directly on acceleration. However, its correlation with damage in building structure is poor, since isolated acceleration peaks hardly affect the structural behaviour.

The Applied Technology Council (ATC, 1984) introduced the concept of effective peak acceleration. Although effective peak acceleration is a philosophically sound parameter for seismic hazard analysis, at present, there is no standardized definition of this parameter. ATC defines the effective peak acceleration (EPA) as follows:

$$\mathrm{EPA} = \frac{\overline{S_{\mathrm{pa}}}}{2.5} \tag{6}$$

where, $\overline{S_{\mathrm{pa}}}$ is the mean pseudo-acceleration value in the period range of 0.1 to 0.5 seconds.

Arias (1970) defined earthquake intensity as the sum of total energy per unit weight stored in the oscillator of a collection of undamped linear oscillators uniformly distributed with respect to their frequencies at the end of duration of earthquake motion, as

$$I_{\mathrm{A}} = (\pi/2g)\int_0^{t_{\mathrm{d}}} \ddot{V}_{\mathrm{g}}^{\,2}(t)\,\mathrm{d}t = (1/2\pi)\int_0^{\infty} \left|F\ddot{V}_{\mathrm{g}}(\varpi)\right|^2 \mathrm{d}\varpi \tag{7}$$

where, t_{d} and $\ddot{V}_{\mathrm{g}}$ are the total duration and ground acceleration of an earthquake; and $\left|F\ddot{V}_{\mathrm{g}}(\varpi)\right|$ is the Fourier amplitude of $\ddot{V}_{\mathrm{g}}(t)$.

Duration of strong motion, as defined by Trifunac and Brady (1975), is

$$t_{\mathrm{d}} = t_{0.95} - t_{0.05} \tag{8}$$

where, $t_{0.05}$ and $t_{0.95}$ are the time t at which I_A has 5% and 95% values, respectively.

Housner (1975) proposed "earthquake power" P_A as a measure of damage potential

$$P_A = \left(1/(t_{0.95} - t_{0.05})\right) \int_{t_{0.05}}^{t_{0.95}} \ddot{V}_g^{\,2}(t)\,dt \tag{9}$$

The root-mean-square of P_A is the measure of average rate of input energy to an elastic system and is defined as

$$\mathrm{RMS}_A = \sqrt{P_A} = \left[\left(1/(t_{0.95} - t_{0.05})\right) \int_{t_{0.05}}^{t_{0.95}} \ddot{V}_g^{\,2}(t)\,dt\right]^{1/2} \tag{10}$$

Housner (1952) also proposed elastic response spectrum intensity (SI)

$$\mathrm{SI}(\xi) = \int_{0.1}^{2.5} S_{pv}(\xi, T)\,dT = \left(1/2\pi\right) \int_{0.1}^{2.5} S_{pa}(\xi, T)\,T\,dT \tag{11}$$

where, T is the period of single-degree-of-freedom oscillator, ξ is the damping ratio, S_{pv} is the pseudo-velocity response spectrum, and S_{pa} is the pseudo-acceleration response spectrum.

Araya and Saragoni (1984) simultaneously have accounted for the effect of maximum amplitude, duration and frequency content (f_0) of strong motion in prescribing earthquake destructive potential factor as

$$P_d = I_A / \mu_0^2 \tag{12}$$

where, I_A is Arias intensity and μ_0 is the frequency of zero crossing.

Table 3: Parameters to Define the Severity of Damage

Event	PGA (g)	EPA (g)	I_A (10^{-1} g.s)	t_d (s)	P_A ($10^{-2}g^2$)	SI (10^{-1}g.s^2)	f_o (Hz)	P_d (10^{-3}g.s^3)
Shock 1 (W-19)	1.470	0.403	1.87	0.18	63.077	2.05	19.60	0.122
Shock 2 (W-20)	1.753	0.474	2.54	0.10	148.54	2.13	18.09	0.194
Shock 3 (W-21)	2.307	0.623	4.54	0.08	354.57	7.07	11.05	0.927
Uttarkashi	0.310	0.225	0.98	6.88	0.82	0.59	5.48	0.816
El Centro	0.348	0.352	1.86	24.44	0.43	0.13	3.09	4.860

Two earthquake ground motions, that is Uttarkashi and El Centro, have been considered for this study. In the shock table records, only main shock has been taken into consideration. Since the weight of shock table is much larger than the weight of model, acceleration history measured at the base of the table are not influenced by the mass and stiffness of the model. The normalized intensity parameters (damage potential factors) for earthquake motion and shock table motion have been determined without any scaling factors and are given in Table 3. The normalization was done by dividing the parameter value by the maximum value in the set. Little correlation is seen to exist among these parameters. Although I_A is also a measure of the energy input to an elastic system, it tends to overestimate the intensity of an earthquake with long duration, high acceleration and frequency content. The spectral intensity SI is also a measure of the damage potential

from an energy stand point because S_{pv} reflects the energy demand of an elastic SDOF system. One obvious disadvantage of the parameter SI is that the duration is not considered, while duration is very important for a structural system experiencing inelastic activity and yielding reversals. The inadequacy of most of these parameters in judging damage intensity arises from the fact that they do not simultaneously consider all the important dynamic characteristics of a ground motion. Table 3 shows that Araya and Saragoni's destructiveness parameter P_d agrees with the observed damage much better than the other parameters because it considers intensity, duration, and frequency content simultaneously.

QUASI-STATIC TESTING OF MODEL

1. Quasi-static Testing

The quasi-static testing consists in applying cyclic load or displacement to the structure at a low frequency so as to represent full range of deformation of the structure under earthquake loading. The slow application of load allows close observation of the structure even when it is cracked as the test progresses. It is the most economical and common method for obtaining information on the inelastic behaviour of structure in which prescribed histories of load or displacement are imposed on the structural system. Such prescribed displacement histories prove to be particularly valuable in (i) assessing the effects of different structural details on the inelastic behaviour of structures by subjecting different specimens to identical deformation histories, and (ii) in studying the basic mechanism that affects the inelastic behaviour of a particular structure by varying the magnitude, rate or pattern of the applied deformation histories. This type of test provides the reversing character of the loading that distinguishes dynamic response from response to uni-directional static loading.

Table 4: Results of Quasi-static Testing of Brick Masonry Houses Models

Parameters of Lateral Resistance					
H_{cr} (kN)	d_{cr} (mm)	H_{max} (kN)	d_{Hmax} (mm)	H_{dmax} (kN)	d_{max} (mm)
28	10.8	36	20	32	25

Stiffness Degradation				
k_e (kN/mm)	k_{Hmax} (kN/mm)	k_{dmax} (kN/mm)	k_{Hmax}/k_e	k_{dmax}/k_e
2.58	1.80	1.28	0.70	0.50

Cumulative Dissipated Energy (kN-mm)		
d_{cr}	d_{Hmax}	d_{max}
150	306	422

Hysteretic Damping (ξ) %		
d_{cr}	d_{Hma}	d_{max}
8.55	6.6	8.35

Ductility Factor (μ)
2.5

H_{max}, d_{max} & μ : Maximum resistance, maximum lateral displacement and ductility factor.

H_{cr} *and* d_{cr} : Force and displacement at the occurrence of the first significant cracks.

k_e, k_{Hmax} & k_{dmax} : Secant stiffnesses at the characteristic points of hysteresis envelops.

2. Test Set-up

Seismic behaviour of brick masonry model has been evaluated by cyclic loading in quasi-static test facility (Agarwal and Thakkar, 1999). The model has been constructed and fixed on the strong floor. The lateral load has been applied by one hydraulic actuator of 10 tons capacity. The maximum stroke is ±150 mm and the flow capacity of the servo-valve is 70 lpm. The actuator is attached to the reaction wall through swivel base and load cell is fixed on the floor diaphragm of the model at mid-section through swivel head. The model is subjected to sinusoidal loading at a frequency of 0.005 Hz under displacement control. Each test consists of two cycles of same loading. The amplitude of loading is increased by 2.5 mm subsequently. The reaction forces at connection between actuator and model are measured by means of load cells, and linear variable differential transformers (LVDTs) are used to measure in-plane and out-of-plane displacement. The walls have been visually inspected and the crack patterns are identified.

3. Discussion of Test Results

The experimental results of the model are analysed in terms of hysteresis behaviour, strength and stiffness degradation, energy dissipation capacity, and mode of failure which have been dealt with in subsequent paragraph (Tomazevic et al., 1993). The results of quasi-static testing are summarized in Table 4.

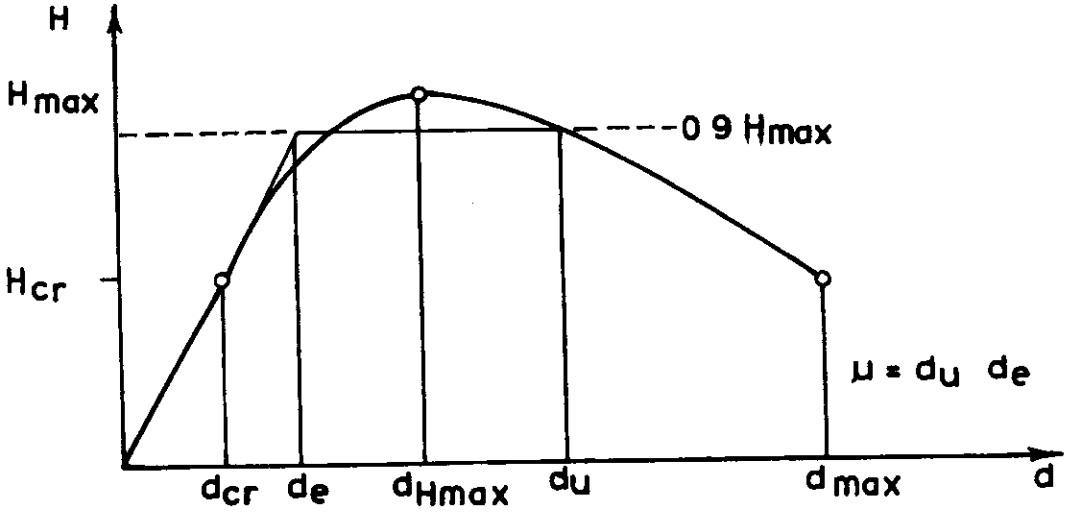

Fig. 6 Parameters of seismic resistance

3.1 Hysteresis Behaviour

The seismic resistance and deformability of the masonry buildings are usually represented by hysteresis behaviour, which shows the relationship between the lateral load acting on the model and lateral deformation. In order to evaluate the parameters which define the seismic behaviour of the walls (maximum resistance H_{max}, maximum lateral displacement d_{max}, and ductility factor μ), the envelopes of hysteresis loops obtained during cyclic test have been plotted (Figure 6) by taking into account the peaks of displacement amplitudes and corresponding resisting forces, such as force and deformation (displacement) at the occurrence of the first significant cracks (H_{cr} and d_{cr}), maximum resistance (H_{max} and $d_{H\,max}$), and maximum lateral displacement (d_{max}). The values are average values obtained in positive and negative directions of loading at a given displacement amplitude. The ductility factor is normally obtained by computing the ratio of d_u and d_e as shown in Figure 6. Since the load deformation curve does not show

clear elastic behaviour in masonry, the same has been computed by the ratio of maximum lateral displacement (d_{max}) and displacement at first cracking of pier (d_{cr}).

The hysteresis curve between applied lateral force versus storey drift has been obtained from the test and it is shown in Figure 7. The behaviour of the model has remained elastic up to a storey drift of 0.3%. Initial cracks have occurred at the storey drift of 1.0%, and maximum lateral strength (H_{max}) equal to 36 kN has occurred at storey drift of 1.25%. The maximum lateral load capacity of models has been computed analytically as 65 kN. The rapid deterioration in lateral load carrying capacity has occurred when storey drift reached 1.50%. The hysteresis curve has not shown clear distinct points at various stages of cracking. The ductility factor obtained from the envelope of hysteresis curve in Figure 8 is nearly 2.5.

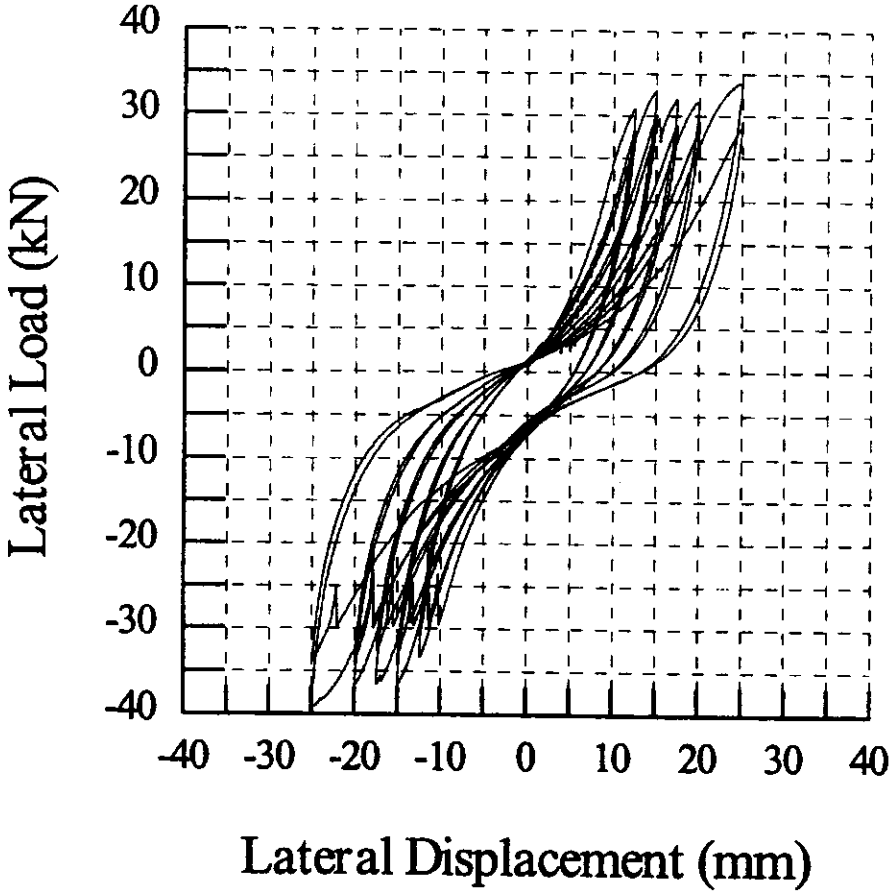

Fig. 7 Hysteresis behaviour (lateral load versus displacement) of model

3.2 Strength and Stiffness Degradation

The average of the absolute values of the extreme positive and negative lateral loads at the first and second cycles at each stage gives an indication of the load degradation at a given displacement level during two consecutive cycles of loading. The stiffness degradation takes place when the models have been subjected to cyclic lateral load reversals. Stiffness degradation has been evaluated on the basis of the measured relationships between the imposed lateral displacements and corresponding reaction forces. Stiffness has been defined as:

$$K_i = \frac{\text{Maximum + ive force} - \text{Maximum} - \text{ive force}}{\text{Corresponding + ive displ.} - \text{Corresponding} - \text{ive displ.}} \tag{13}$$

In order to compare the degree of stiffness degradation, the calculated values are also expressed in terms of the initial effective stiffness of the models.

It has been observed from the hysteresis curve that there is a perceptible decrease in stiffness. This was observed as the storey drift increased from first cracking to the maximum lateral displacement. Initial stiffness of the models decreased from 50 to 70% as the storey drift increased from 0.30 to 1.5%. The decrease in stiffness occurred due to diagonal cracking, and brick and mortar crushing.

3.3 Energy Dissipation Capacity and Hysteretic Damping

As a measure of energy dissipation capacity (EDC) at a given displacement amplitude, cumulative input energy has been compared with dissipated hysteretic energy. Cumulative input energy E_{inp} has been defined as the cumulative work of the actuator, needed to deform the specimen from the beginning of test to the given displacement amplitude. Work of the actuator needed to deform, that is to push and pull the model to maximum displacement amplitudes in one cycle of loading, is calculated as the sum of areas under the positive and negative parts of hysteresis loop. The amount of dissipated energy E_{diss} in one cycle of loading has been defined and calculated as the area of hysteresis loop between two consecutive displacement peaks.

$$\text{EDC} = \frac{\text{Energy Dissipated/Cycle}}{\text{Total Stored Energy/Cycle}} \tag{14}$$

The average values of coefficient of hysteretic damping in one cycle of loading are calculated at the characteristic points of hysteresis envelope,

$$\zeta = (1/2\pi)\left(\frac{\text{Energy Dissipated/Cycle}}{\text{Total Stored Energy/Cycle}}\right) \tag{15}$$

It has been observed from the hysteresis curve that the rate of energy dissipation is gradually increasing up to a storey drift of 0.75%, but after attaining the maximum lateral state, the energy dissipation sharply increases. The energy dissipated during the hysteresis loop at maximum lateral displacement is about 50% of input energy. The damping obtained from the hysteretic curve is around 7%, which is more in comparison to the damping obtained from the free vibration test (6%).

3.4 Inelastic Behaviour and Mode of Failure

The sequence of horizontal displacements continues until failure stage of the model is not reached. The shear failure of the piers between lintel and sill bands has been observed by the initiation of visible cracking along the pier diagonals, when the principal tensile stresses exceeded the tensile strength of masonry under increasing imposed horizontal displacements. These diagonal cracks opened extensively, resulting in a major X-shaped diagonal crack pair and thus leading to a relatively sudden and destructive failure. This type of failure is called "brittle shear failure". These cracks initiated from the N-E corner of the opening and reached diagonally the opposite corner of the sill band.

A shear-sliding mode of failure has been observed in the piers below the sill band. The cracking has occurred at the ends of the top end of sill band and bottom of model where the tensile stresses due to flexure have remained the greatest. Diagonal cracking also has taken place at a later stage as the horizontal load increased. A sliding failure started over the cross-section in the form of a wide horizontal cracking. The main characteristic of the sliding mode of failure is the lack of diagonal tension (shear) cracks on the face of piers. The cracks, which were horizontal, initiated at the top and bottom of the piers and propagated through the full cross-section, leaving the rest of the pier undamaged.

Out-of-plane mode of failure has not been observed in either of the cross-walls. The main reason is the laying of earthquake resistant provision, i.e. roof slab with lintel and sill bands and corner and jamb steel which restricted the out-of-plane failure completely. Only a few horizontal cracks developed in both the cross-walls of the models. The cracking remained mainly confined between lintel and sill levels.

COMPARISON BETWEEN STATIC AND DYNAMIC RESPONSE OF MODEL

A study has been made here to compare the behaviour of two masonry models constructed with identical strengthening features under two types of testing. The criterion for comparison is the maximum displacement measured at the roof level in shock test and corresponding displacement in quasi-static test. The purpose of studying correlation between shock table testing and quasi-static testing is to suggest differences in strength and stiffness in each method and to study correlation between inelastic and cracking behaviour of models near failure state.

Table 5: Comparison of Results in Shock Test and QST of Model

Shock No.	d_T (mm) QST	d_T (mm) Shock test	F_T (kN) QST	F_T (kN) Shock table result	Stiffness (K) kN/mm
1	12.5	12.78	32.5 (80%)	40.0	2.6 (81%)
2	15	15.53	34.0 (70%)	48.2	2.26 (70%)
3	17.5	17.46	32.0 (67%)	46.0	1.82 (66%)

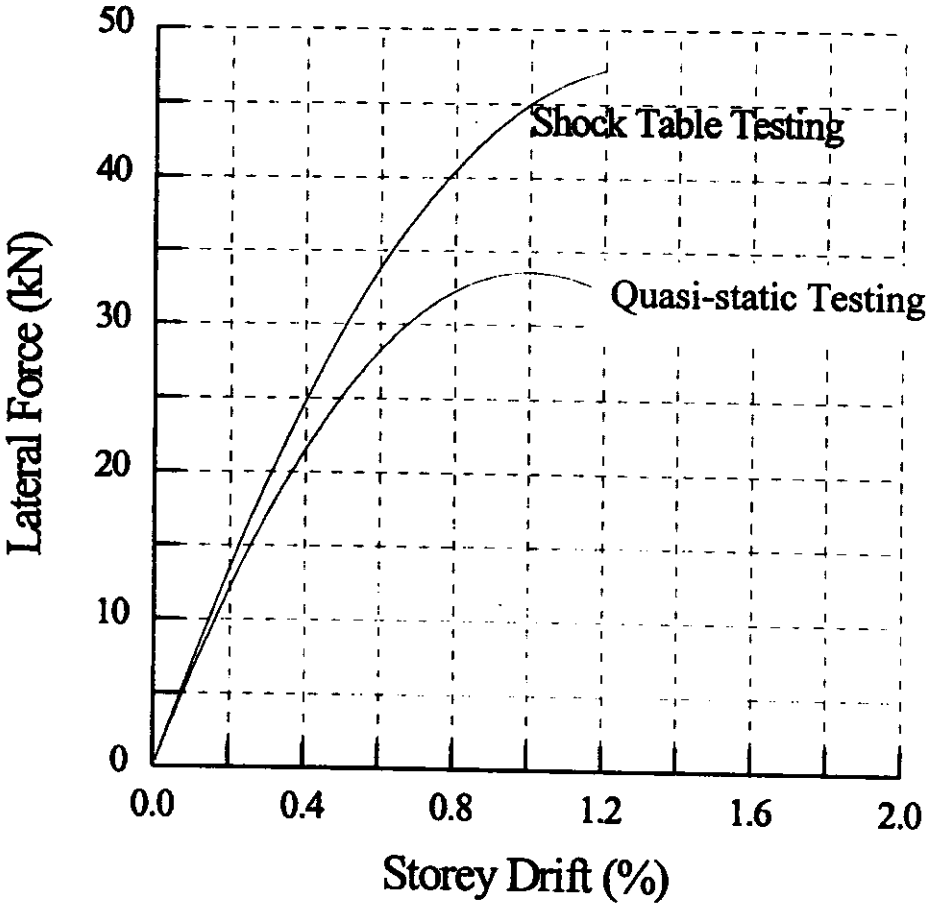

Fig. 8 Equivalent lateral load deformation envelope curves

The load deformation envelope curve of model under quasi-static testing and shock table testing has been presented in Figure 8. Marked reductions in both strength and stiffness have been observed when the model is loaded statically rather than dynamically. The variation in percentage of corresponding values of maximum response as measured with dynamic test, for each is presented in Table 5. Significant differences in stiffness have been observed at the beginning of the test and little difference may be observed once the structure is cracked. Therefore, a structure subjected to dynamic loading responds with a significantly higher initial strength and stiffness than other structure, which is subjected to the same history of lateral deflections under static condition.

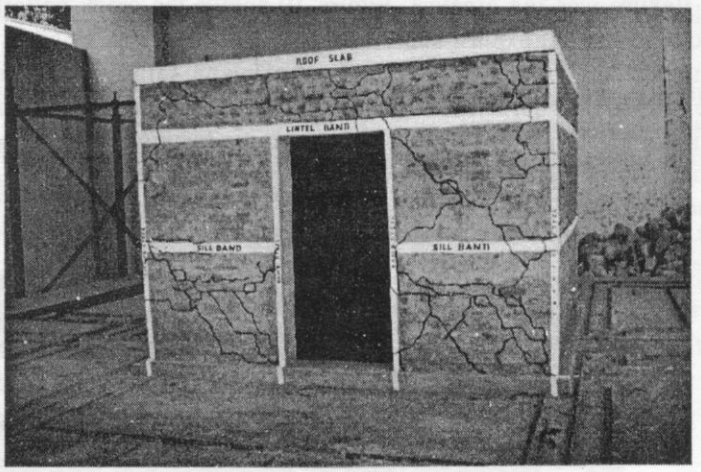

(a) Crack pattern of south shear wall in shock table tests

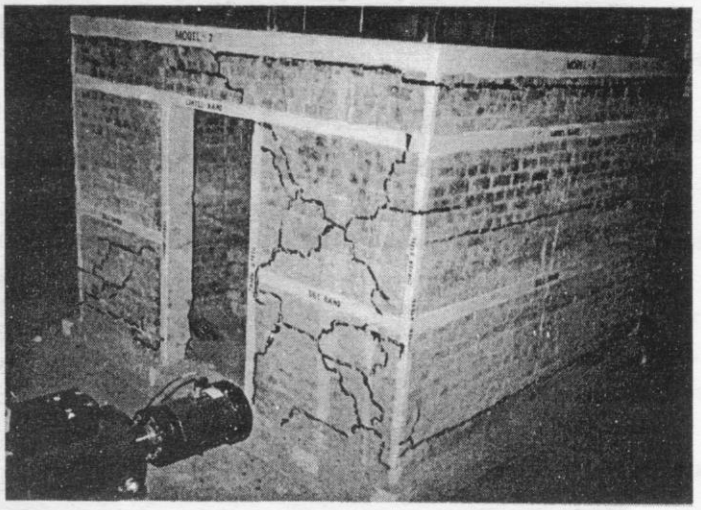

(b) Crack pattern of south shear wall in quasi-static tests

Fig. 9 Crack patterns of south shear wall of model

The crack pattern obtained under both the test methods is nearly similar. The piers of south shear wall failed nearly in the same manner under both types of testing. A shear failure has been observed in the right side of pier between lintel and sill bands while left-side pier has almost remained undamaged under both the testings. The right pier below the sill band failed in the mode of ductile shear failure, while the left pier under shock test failed in combined shear and flexure mode and the same pier in quasi-static test failed in flexure mode. Figure 9 shows the crack pattern in south shear wall of model in shock test and quasi-static test. The right piers between the lintel and sill bands of north shear wall of the model indicate shear mode of

failure. This is characterised as double diagonal in quasi-static test, and single diagonal under shock test. This is because the model under quasi-static test was subjected to reversible-type cyclic loading, while in shock table test, the duration of shock motion was very short. The wall had only been subjected to one or two significant loading reversals, which is manifested by the signature of shock table motion. The pier below the sill band failed in combined shear and sliding mode under both types of the testing. In shock test, the initial cracking started in the form of horizontal (flexure) cracks at the bottom corners of the piers, which later became diagonal (inclined) cracks. In quasi-static test, this mode of failure has been characterised by the diagonal cracking at the top and bottom ends of the pier. This has then continued horizontally where the tensile stress due to flexure was the greatest. Figure 10 shows the crack pattern in the north shear wall of model in both the shock test and the quasi-static test. No significant cracking has been observed in the cross - wall of the model under both the testings. The out-of-plane failure has been almost totally restricted. Visually, the damage in model under dynamic testing happens to be less than that observed under quasi-static condition. Thus, the model testing reveals that the quasi-static testing is a conservative approach to determine the response quantities as compared to the shock table testing, in the absence of vertical acceleration and simultaneous in-plane and out-of-plane action.

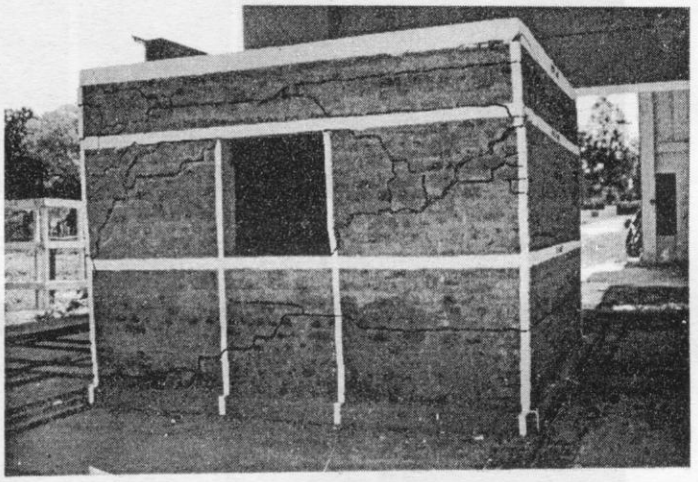

(a) Crack pattern of north shear wall in shock table tests

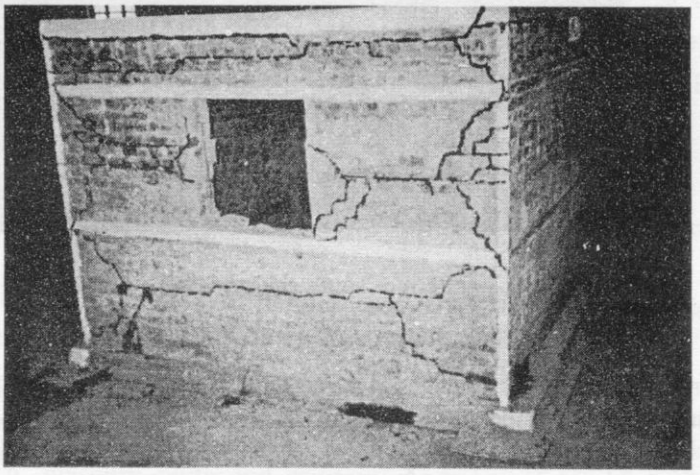

(b) Crack pattern of north shear wall in quasi-static tests

Fig. 10 Crack patterns of north shear wall of model

CONCLUSIONS

A comparison has been presented to demonstrate the differences in the behaviour of brick masonry model subjected to either shock table motion or quasi-static loading. The important conclusions of this study are as follows.

The shock table model responds with a significantly higher initial strength and stiffness as compared to the quasi-static model subjected to equivalent lateral displacements. It has been observed that the severity of damage is greater in quasi-static test due to increased crack propagation.

The lateral load parameters of brick masonry model as determined by quasi-static testing are conservative compared to the dynamic testing.

The shock test suggests that at low levels of excitation at the base, acceleration gets amplified at the roof, with an almost elastic behaviour of the model. This amplification tends to decrease as the test sequence continues. This indicates that the damaged lower part of the model functions as a kind of base isolator, which prevents propagation of energy into upper portion of structure.

The experimental tests reveal that the brick masonry models behave elastically up to a storey drift of 0.30%. The ductility of brick masonry models is observed to be around 2.5.

The experimental tests reveal that the piers of the model between lintel and sill bands fail in brittle shear mode while the piers below sill band fail in ductile shear mode. The out-of-plane failure is considerably improved by providing the earthquake resistant measures.

REFERENCES

1. Agarwal, P. (2000). "Experimental Study of Strengthening and Retrofitting Measures in Masonry Buildings", Ph.D Thesis, Department of Earthquake Engineering, University of Roorkee, Roorkee.
2. Agarwal, P. and Thakkar, S.K. (1999). "Quasi-static Testing of Seismically Strengthened Brick Masonry Models", International Symposium on Theory and Application of Structural Engineering Test Method, Dept. of Civil Engineering, Tsinghua University, China.
3. Arya, A.S. and Kumar A. (1982). "An Earthquake Resistant as Well as Economical Brick Building System", 7th Symposium on Earthquake Engineering, Roorkee.
4. Araya, R. and Saragoni, G. (1984). "Earthquake Accelerogram Desstructiveness Potential Factor", Proceedings of the Eighth World Conference on Earthquake Engineering, San Francisco, California, U.S.A., pp. 835-842, Prentice-Hall, Inc., New Jersey, U.S.A.
5. Arias, A. (1970). "A Measure of Earthquake Intensity", Seismic Design for Nuclear Power Plants (Ed. R.J. Hansen), pp. 438-469, The M.I.T. Press, Cambridge, Massachusetts, and London, England.
6. ASTM: E 447-84 (1984). "Compressive Strength of Masonry Assemblage", American Society of Testing and Materials, Philadelphia, U.S.A.
7. ASTM: E 72 (1989). "Standard Methods for Conducting Strength Tests on Panels for Building Construction", American Society of Testing and Materials, Philadelphia, U.S.A.
8. ATC-3-06 (1984). "Tentative Provisions for the Development of Seismic Regulation of Buildings", Technical Report, Applied Technology Council, 555 Twin Dolphin Drive, Suite 550, Redwood City, California, U.S.A.
9. Benedetti, D. and Castellani, A. (1982). "Dynamic and Static Experimental Analysis of Stone Masonry Buildings", Proceedings of 7th ECEE, Athens, Greece.
10. Clough, R.W., Mayes, R.L. and Gulkan, P. (1979). "Shaking Tables Study of Single Storey Masonry Houses - Volume 3: Summary, Conclusions and Recommendations", Report No. UCB/ EERC 79/25, Earthquake Engineering Research Centre, University of California at Berkeley, U.S.A.
11. Drysdale, R.G., Hamid, A.A. and Baker, L.R. (1994). "Masonry Structures Behaviour and Design", Prentice Hall, Englewood Cliffs, New Jersey, U.S.A.

12. Housner, G. (1975). "Measures of Severity of Earthquake Ground Shaking", Proceedings of the U.S. National Conference on Earthquake Engineering, pp. 25-33, Earthquake Engineering Research Institute, Ann Arbor, Michigan, U.S.A.
13. Housner, G. (1952). "Spectrum Intensities OF Strong Motion Earthquakes", Proceedings of the Symposium of Earthquake and Blast Effects on Structures, pp. 21-36, Earthquake Engineering Research Institute, Los Angles, California, U.S.A.
14. IS: 13928 (1993). "Improving Earthquake Resistance of Low Strength Masonry Buildings - Guidelines", Bureau of Indian Standards, New Delhi.
15. Krishna, J. and Chandra, B. (1965). "Strengthening of Brick Buildings against Earthquake Forces", 3rd World Conference on Earthquake Engineering, New Zealand.
16. Keightley, W.O. (1977). "Report on Indo-U.S. Sub-commission on Education & Culture", Department of Earthquake Engineering, University of Roorkee, Roorkee.
17. Meskouris, K. (1996). "Dynamics of Civil Engineering Structures", A.A. Balkema, Rotterdam, Netherlands.
18. Paulay, T. and Priestley, M.J.N. (1992). "Seismic Design of Reinforced Concrete and Masonry Buildings", John Wiley & Sons, Inc., U.S.A.
19. Paulson, T. J. and Abrams, D. P. (1990). "Correlation between Static and Dynamic Response of Model Masonry Structures", Earthquake Spectra, Vol. 12, No. 1.
20. Qamaruddin, M. (1978). "Development of Brick Building System for Improved Earthquake Performance", Ph.D. Thesis, Department of Earthquake Engineering, University of Roorkee, Roorkee.
21. Tomazevic, M. and Velechovsky. T. (1992). "Some Aspects of Testing Small-Scale Masonry Buildings Models on Simple Earthquake Simulators", Earthquake Engineering and Structural Dynamics, Vol. 21, pp. 945-963.
22. Tomazevic, M. and Lutman, M. (1993). "In Plane Behaviour of Reinforoed Masonry Walls Subjected to Cyclic Lateral Loads Part Two: Analysis of Test Results", Report ZRMK/ PI-92/08, Ljubljana, Slovenia.
23. Trifunac, M. and Brandy, A. (1975). " A Study on the Duration of Strong Earthquake Ground Motion", Bull. Seism. Soc. Am., Vol. 65, pp. 581-626.
24. Turnsek, V. and Cacovic, F. (1970). "Some Experimental Results on the Strength of Brick Masonry Walls", Proceedings of 2nd International Brick Masonry Conference, British Ceramic Society, Stoke-on-Trent, U.K., pp. 149-156.
25. Uang, C.-M. and Bertero, V.V. (1988). "Implications of Recorded Earthquake Ground Motions on Seismic Design of Building Structures", Report No. UCB/EERC-88/13, University of California, Berkeley, CA, U.S.A.